Reading and writing charge on graphene devices

M. R. Connolly,[1,2] E. D. Herbschleb,[1] R. K. Puddy,[1] M. Roy,[3] D. Anderson,[1] G. A. C. Jones,[1] P. Maksym,[3] and C. G. Smith[1]
[1]*Cavendish Laboratory, Department of Physics, University of Cambridge, Cambridge CB3 0HE, United Kingdom*
[2]*National Physical Laboratory, Hampton Road, Teddington TW11 0LW, United Kingdom*
[3]*Department of Physics and Astronomy, University of Leicester, University Road, Leicester LE1 7RH, United Kingdom*

(Received 25 October 2011; accepted 19 June 2012; published online 11 July 2012)

We use a combination of charge writing and scanning gate microscopy to map and modify the local charge neutrality point of graphene field-effect devices. We give a demonstration of the technique by writing remote charge in a thin dielectric layer over a graphene-metal interface and detecting a shift in the local charge neutrality point. We perform electrostatic simulations to characterize the interaction between a realistic scanning probe tip, the deposited charge, and the graphene and find a good semi-quantitative agreement with the experimental results. © *2012 American Institute of Physics*. [http://dx.doi.org/10.1063/1.4732802]

Gate tuneable conductivity underpins the operation of a multitude of applications envisaged for graphene, ranging from switching in mass-produced field-effect transistors to single electron manipulation in quantum dots. Topographic, morphological, and electrostatic variability often compromises device performance, so developing tools for imaging and modifying local electronic properties continues to receive considerable interest. Charge writing (CW) uses the biased tip of a scanning probe microscope to deposit charge in a dielectric layer electrostatically coupled to a nanodevice, so far mainly those fabricated from two-dimensional electron gas-based systems in semiconductor heterostructures,[1,2] and scanning gate microscopy (SGM) employs the same tip as a mobile gate for imaging the charge-induced changes in local conductivity. While SGM has also recently proven capable of making charge neutrality point (CNP) maps of inhomogeneously doped graphene flakes,[3,4] combined CW/SGM has not been performed to control the electronic properties of graphene devices. In this letter we both measure and modify the local CNP of a graphene flake using SGM and CW, paving the way towards electrostatic lithography of graphene devices. We also perform self-consistent electrostatic simulations that account for the realistic geometry of the tip and the bandstructure of graphene and show that a scanning probe tip induces potential perturbations in the graphene on both the micron- and tip-apex scale.

Our graphene devices are fabricated from flakes which are mechanically exfoliated from natural graphite onto a highly doped Si substrate capped with a 300 nm thick SiO_2 layer. The number of layers is identified from their optical contrast and 5/30 nm Ti/Au contacts are patterned using e-beam lithography, thermal evaporation, and standard poly methyl methacrylate (PMMA) lift-off processing. For improved stability and sensitivity we operate our scanning probe microscope in non-contact mode (see Ref. 3 for details) and under vacuum (10^{-5} mbar) with an average tip-surface separation of 5–20 nm. The SGM setup used to image the CNP is shown in Fig. 1(a). To benefit from the high signal-to-noise ratio achievable using a.c. detection, we modulate the voltage V_T on the tip (NanoWorld ARROW-NCPt) at low frequency (typically 3 V at 1 kHz) and detect the modulation of I_{DS} ($\approx$250 μA) using a lock-in amplifier. The demodulated component δI_{DS} is proportional to the local transconductance $g_m = \partial I_{DS}/\partial V_T$ ($\approx 0.2\,\mu$A/V).[3,5] Our earlier work established that the back-gate voltage which nulls the transconductance is the local charge neutrality point (V_0), and spatial maps of V_0 were generated by performing point spectroscopy and extracting V_0 at each point.[3] Point measurements are necessary as raw SGM data reflects variations in both mobility and carrier density, making it difficult to extract one or the other from a single image. Owing to the sign change of the transconductance either side of V_0, $g_m(V_{BG})$ is highly suited as an error signal which can be nulled in a feedback loop for real-time tracking of V_0. This avoids the need to perform point measurements and is similar to the real-time compensation of the contact potential used in scanning Kelvin probe microscopy.[6] Fig. 1(a) shows the circuit used to implement "nulling" scanning gate microscopy (NSGM). The modulation in current δI_{DS} is fed into a software controlled feedback loop which adjusts the back-gate voltage to maintain a constant setpoint $\delta I_{DS}(V_0) = 0$. Fig. 1(c) shows a map of V_0 captured using NSGM in four-terminal configuration on a bilayer flake with a bulk neutrality point at $V_{BG} \approx -4$ V. The greatly improved resolution and capture time ($\approx$10 min) allows us to observe up to 2 V variations in V_0, mostly due to the pronounced *n*-type doping around the Ti/Au contacts. Line profiles shown in Fig. 1(d) show that the doping extends hundreds of nanometers away from the contacts. We have performed NSGM on other flakes in both two and four terminal configurations and observe similar doping profiles around contacts, in good agreement with various microscopy studies[7–9] and theoretical analyses taking into account the different work functions of graphene and titanium.[10]

The features in the NSGM images shown in Fig. 1(c) vary over hundreds of nanometers, indicating a large effect from the conical section of the tip. This is not unexpected as the tip used in these experiments has a relatively large half-

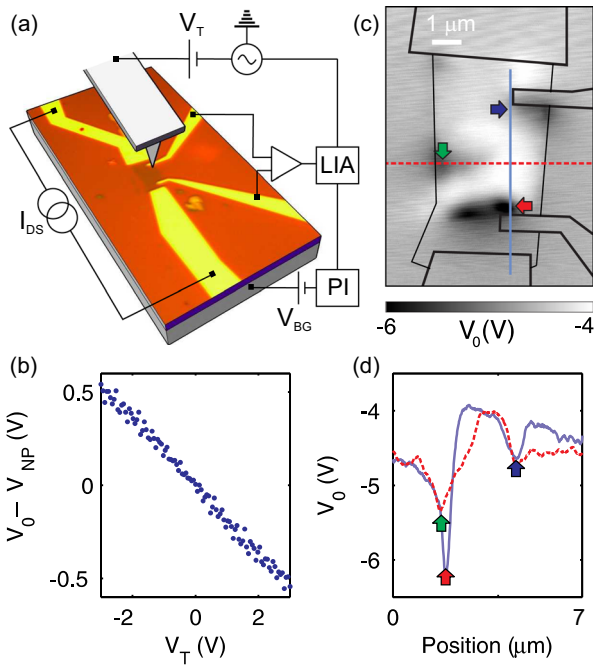

FIG. 1. (a) Circuit used to perform nulling scanning gate microscopy in four-terminal configuration on a graphene bilayer [LIA: lock-in amplifier, PI: proportional-integral controller]. (b) Difference between the nulling back-gate voltage and the bulk neutrality point voltage as a function of d.c. voltage applied to the tip. (c) Map of the neutrality point V_0 of the graphene bilayer shown in (a). (d) Horizontal (dashed) and vertical (solid) line profiles. Arrows correspond to the *n*-type doping features indicated in the map.

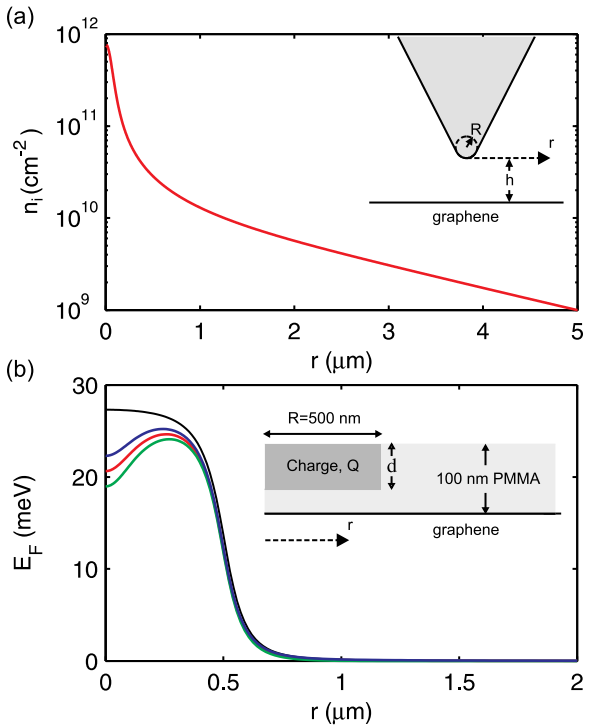

FIG. 2. (a) Main figure: calculated induced electron density as a function of horizontal distance r from the tip apex. Inset: schematic of tip geometry ($h = 20$ nm). The tip is modelled as a blunt cone with an opening angle of 30° and a spherical end with $R = 100$ nm as shown. (b) Main figure: calculated $E_F(r)$ due to a charge deposited in PMMA, with $d = 50$ nm and $Q = 7400$ e. Solid black line: in the absence of the AFM tip. Coloured lines: in the presence of the AFM tip at $h = 120$ nm above the bilayer graphene. Red: $V_T = 0$ V, blue: $V_T = -1$ V, green: $V_T = +1$ V. Inset: schematic of the geometry of the PMMA layer and the cylindrical region of uniform charge density.

cone angle $\theta_0 \approx 30°$, which starts to dominate for tip-surface separations ≥ 5 nm.[11,12] A similar long-range SGM response was reported in the context of SGM on carbon nanotubes[11] and subsurface two dimensional electron gases,[13,14] where it was distinguished from finer conductance variations which occur on the scale of the tip apex.[14]

In addition to the length scale of the perturbation, an important parameter characterizing SGM is the carrier density induced under the tip, which can be quantified through the effective capacitive coupling $\beta = \Delta n/V_T$, where Δn is the change in carrier density under the tip. NSGM enables us to measure β directly by sweeping the DC voltage applied to the tip and tracking the nulling back-gate voltage. Fig. 1(b) shows a plot of the difference between the nulling voltage and the bulk neutrality point voltage (V_{NP}) captured as a function of V_T with the tip held above the middle of the device in Fig. 1(c). Using the known relationship between carrier density and back-gate voltage, $n = \alpha(V_{BG} - V_{NP})$ ($\alpha = 7.2 \times 10^{10}$ cm^{-2}),[15] we infer a coupling between the tip and the graphene of $\beta \approx 13 \times 10^9$ cm^{-2}/V.

To obtain a theoretical estimate for the length scale and coupling strength of the tip perturbation, we solve Laplace's equation numerically in cylindrical polar co-ordinates for a realistic tip-sample geometry. We include the screening charge induced in the graphene self-consistently within the Thomas-Fermi approximation. In our model, a blunt tip (see inset to Fig. 2) is positioned 20 nm above a clean, homogeneous bilayer graphene sheet which lies on a 300 nm thick dielectric substrate. Experimentally, we are close to the neutrality point, so in our idealized model, we fix the voltage at the bottom of the substrate to 0 V. At the upper boundary of the dielectric, the electric displacement is discontinuous by an amount determined by the charge density induced in the bilayer. We calculate this self-consistently. The Fermi level, $E_F(r)$, in the bilayer varies spatially with the voltage in the graphene and the induced charge density, $n_i(r) = \gamma_1(E_F(r) - E_g(r)/2)/(\pi P^2)$ for $E_F > E_g/2$, is derived from the low energy parabolic dispersion for a bilayer.[16] Here, $P = 0.539$ eV nm,[17,24,26,27] $\gamma_1 = 0.39$ eV,[16] and $E_g(r) = [e^2V_{bl}^2\gamma_1^2/(e^2V_{bl}^2 + \gamma_1^2)]^{1/2}$ is the band gap induced in the bilayer[18] due to the bias, V_{bl}, across it.[25]

The calculated charge density is shown in Fig. 2(a). In our calculation we extend the system in radial (to $r = 50\,\mu$m) and vertical (to $z = 6.3\,\mu$m) directions until $n_i(r)$ is converged to within 0.05% for $r < 5\,\mu$m. Qualitatively, $n_i(r)$ is not sensitive to the band-structure model. Even changing the bilayer to monolayer graphene has an effect of less than 2% under the tip.[25] Instead, it is the tip shape and V_T that primarily determine $n_i(r)$. Within $r < 5\,\mu$m we find that the charge density is well fitted by the sum of two Lorentzians, one which is broad and shallow, and one which is narrow and deep. The Lorentzian peak height varies linearly with V_T, but the half widths are insensitive to tip voltage and vary by $< 1\%$ for $0.5 \leq V_T \leq 3$ V. At $V_T = 3$ V the wider of the Lorentzians has a peak height, $n_i(0) = 14 \times 10^9$ cm^{-2}, and a half width of $3.6\,\mu$m, which fits well with the observed micron-sized perturbation and gives a value for $\beta = \Delta n/V_T = n_i(0)/V_T \approx 5 \times 10^9$ cm^{-2}/V, similar to that

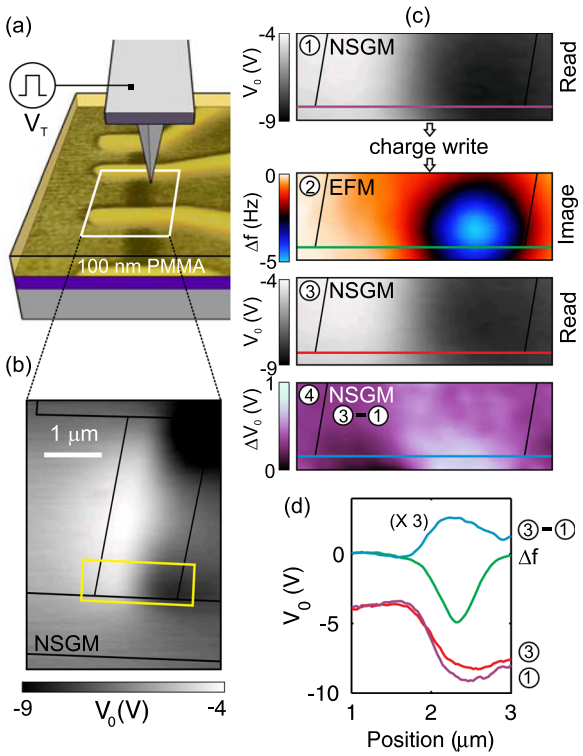

FIG. 3. (a) Setup used to write charge in a 100 nm thick layer of PMMA spin-coated over the graphene. Voltage pulses ($20\,V_{Pk-Pk}$ at 50 Hz) are applied to the tip in tapping mode to write charge. (b) Nulling scanning gate micrograph showing the charge neutrality point distribution prior to writing. (c) Procedure for combining NSGM with charge writing to sequentially read and write charge neutrality point distributions over graphene devices. (d) Line profiles of the neutrality point and frequency shift for the NSGM and EFM images, respectively.

found experimentally. The factor of ≈3 discrepancy probably stems from the uncertainty in the characteristic area under the tip apex where the local charge density must be neutralized in order to null the transconductance. Since the size of features in the NSGM images are broad, in our estimate for β we select the density at the peak $n_i(0)$ of the broad Lorentzian as the one that needs to be compensated. However, it is probable that the tip must also partially neutralize the narrow and deep perturbation, which has a much higher apex carrier density.[19,20] An approximate characterization of the effect of the tip can also be made by estimating the effective radius, R, of a parallel plate capacitor which yields the experimentally determined β. From the simulated charge density shown in Fig. 2(a), we calculate $Q(R) = 2\pi\int_0^R n_i(r')r'dr'$. Then, $\beta(R) = Q(R)/(\pi R^2)/V_T \approx 13 \times 10^9\,\mathrm{cm}^{-2}$ for an effective radius of $R \approx 700$ nm.

We now show how the tip can be employed to modify the CNP map by performing CW to induce holes in the graphene and partially compensate for the *n*-type doping around the contacts. We spin coated a 100 nm thick layer of PMMA to act as the CW dielectric over the device shown in Fig. 3(a). Fig. 3(b) shows the NSGM map in the presence of the PMMA layer. Note the reduced spatial resolution due to the necessity of scanning ≈100 nm from the surface and the enhanced *n*-type doping, especially next to the contacts where V_0 reaches as low as ≈ −9 V. Further work is required to optimize the use of thinner and less invasive dielectrics. Prior to CW we acquire a higher resolution NSGM image of $V_0(x, y)$ next to the contacts [Fig. 3(c), image 1]. To perform CW in PMMA we follow the procedure presented in Ref. 21 for creating electrostatic templates. The tip is brought in to hard tapping-mode contact over the doped region and a square-wave signal between −10 and −30 V at 50 Hz is applied to the tip. These values bring the pulses over the ≈15 V threshold pulse amplitude for charge deposition in PMMA.[21] As expected in tapping mode and pulsed writing, topographic imaging did not show any subsequent damage to the PMMA and worked equally well with depositing positive and negative charges.[21] For imaging the deposited charge we employ electrostatic force microscopy (EFM) and Kelvin probe microscopy (KPM) when quantitative estimates of the surface potential are required. To eliminate the well known interference between potential variations and topographic features in scanning probe measurements, we perform both techniques using a dual-pass configuration. The surface topography is recorded in tapping mode during the first pass. In the second pass the topographic data is used to keep the tip withdrawn 100 nm from the surface while the frequency shift or nulling voltage is recorded, giving a more accurate electrostatic measurement. An EFM image showing the shift in frequency (Δf) of the cantilever over the charged region is shown in Fig. 3(c), image 2. The charge is well localized and corresponds to a surface potential of ≈ −2 V as measured using KPM. We re-map V_0 in NSGM after CW (Fig. 3(c), image 3) and construct the difference (Fig. 3(c), image 4) to enhance the CNP shift. Line profiles in Fig. 3(d) show a good correspondence between the peaks of written charge and the CNP shift, which is ≈0.8 V. We found the charge to be stable for several days under vacuum at room temperature, in good agreement with previous observations.[21]

From the measured CNP shift of $\Delta V_0 \approx 0.8$ V and the dependence $E_F = (\pi\hbar^2/2m^*)\alpha\Delta n$ for bilayer graphene, where the effective mass m^* is related to the electron mass m_e by $m^* \approx 0.03m_e$,[22] we deduce that the Fermi level shifts by around ≈25 meV below the written charge pattern. Using our simulation together with this shift in E_F, we can estimate the amount of charge deposited into the PMMA. In our model we add a 100 nm layer of PMMA dielectric ($\varepsilon_r = 2.89$) above the bilayer graphene. We introduce some charge into this PMMA layer, and, for simplicity, we assume that the charge density, ρ, is uniform. The charge is deposited within a cylindrical volume of radius $r = 500$ nm down to a depth d below the surface of the PMMA, so that the total written charge is $Q = Ne = (\pi r^2 d)\rho$, where N is the total number of electron charges, e. In our simulations we vary N and d, solve Poisson's equation self consistently as before, and search for a shift in E_F of ≈25 meV directly below the written charge pattern. There is no unique solution for N and d: a larger number of charges localized near to the top surface of the PMMA will have the same effect on E_F as a smaller number of charges spread throughout the PMMA layer. However, from our numerical results, we find that $N \approx N_0 - ad$ is the total number of charges required to raise E_F by 25 meV, where $N_0 \approx 7600$, $a \approx 5\,\mathrm{nm}^{-1}$, and $d \leq 0 \leq 100$ nm. As there is some uncertainty in our estimate of E_F we have repeated the calculation for 20 meV

$\leq E_F \leq 30$ meV. Within this range the total deposited charge is roughly proportional to E_F. Changing our estimate for E_F by ± 5 meV alters N_0 by ± 1500 and has relatively little effect on a. These conclusions are consistent with previous estimates which assume the charge is distributed throughout the PMMA,[23] highlighting the potential of graphene for characterizing the nature of charge injection and nanopatterning of a wide range of dielectric materials.

Fig. 2(b) (solid black line) shows the Fermi level of the bilayer graphene as a function of r when $N = 7400$ and $d = 50$ nm. Fig. 2(b) also illustrates the sensitivity of E_F to the AFM tip in the presence of the written charge. When the tip is absent or very far from the PMMA surface, the electric field around the deposited charge decays slowly with height. However, when the tip is brought close to the surface the electric field above the PMMA must go rapidly to zero, with the net result that the potential inside the PMMA layer (and hence in the bilayer graphene) is reduced. The coloured lines in Fig. 2(b) show this effect: the Fermi level tends to be reduced in the presence of the tip, but can be adjusted by varying the tip voltage, V_T.

In conclusion, we have introduced a method which combines charge writing and scanning gate microscopy to read and write the local charge neutrality point on a graphene device. We mapped the variation of doping across a bilayer flake and found micron-sized n-type doping from Ti/Au contacts. We performed electrostatic simulations to analyze the interaction between the biased tip, the deposited charge, and the graphene and deduced an effective capacitive coupling of $\beta \approx 5 \times 10^9\ \mathrm{cm}^{-2}/\mathrm{V}$, which is in reasonable quantitative agreement with the value determined experimentally. We deposited charge with a surface potential of ≈ -2 V and shifted the CNP of a region next to the metallic contacts by ≈ 0.8 V. The use of thinner, less invasive dielectrics with higher permittivity would improve the technique and enable the *in situ* fabrication of graphene devices with arbitrary potential landscapes.

[1]R. Crook, A. C. Graham, C. G. Smith, I. Farrer, H. E. Beere, and D. A. Ritchie, Nature (London) **424**, 751 (2003).
[2]R. Crook, J. Prance, K. J. Thomas, S. J. Chorley, I. Farrer, D. A. Ritchie, M. Pepper, and C. G. Smith, Science **312**, 1359 (2006).
[3]M. R. Connolly, K. L. Chiou, C. G. Smith, D. Anderson, G. A. C. Jones, A. Lombardo, A. Fasoli, and A. C. Ferrari, Appl. Phys. Lett. **96**, 113501 (2010).
[4]R. Jalilian, L. A. Jauregui, G. Lopez, J. Tian, C. Roecker, M. M. Yazdanpanah, R. W. Cohn, I. Jovanovic, and Y. P. Chen, Nanotechnology **22**, 295705 (2011).
[5]R. Crook, C. G. Smith, C. G. Simmons, and D. A. Ritchie, J. Phys.: Condens. Matter **12**, L735 (2000).
[6]M. Nonnenmacher, M. P. O'Boyle, and H. K. Wickramasinghe, Appl. Phys. Lett. **58**, 2921 (1991).
[7]E. J. H. Lee, K. Balusubramanian, R. T. Weitz, M. Burghard, and K. Kern, Nat. Nanotechnol. **3**, 486 (2008).
[8]T. Mueller, F. Xia, M. Freitag, J. Tsang, and P. Avouris, Phys. Rev. B **79**, 245430 (2009).
[9]Y.-J. Yu, Y. Zhao, S. Ryu, L. E. Brus, K. S. Kim, and P. Kim, Nano Lett. **9**, 3430 (2009).
[10]P. Khomyakov, A. Starikov, G. Brocks, and P. Kelly, Phys. Rev. B **82**, 115437 (2010).
[11]N. R. Wilson and D. H. Cobden, Nano Lett. **8**, 2161 (2008).
[12]S. Hudlet, M. S. Jean, C. Guthmann, and J. Berger, Eur. Phys. J. B **2**, 5 (1998).
[13]A. Baumgartner, T. Ihn, K. Ensslin, G. Papp, F. Peeters, K. Maranowski, and A. C. Gossard, Phys. Rev. B **74**, 165426 (2006).
[14]M. G. Pala, B. Hackens, F. Martins, H. Sellier, V. Bayot, S. Huant, and T. Ouisse, Phys. Rev. B **77**, 125310 (2008).
[15]K. S. Novoselov, A. K. Geim, S. V. Morozov, D. Jiang, Y. Zhang, S. V. Dubonos, I. V. Grigorieva, and A. A. Firsov, Science **306**, 666 (2004).
[16]E. McCann and V. I. Fal'ko, Phys. Rev. Lett. **96**, 086805 (2006).
[17]D. P. Di Vincenzo and E. J. Mele, Phys. Rev. B **29**, 1685 (1984).
[18]E. V. Castro, K. S. Novoselov, S. V. Morozov, N. M. R. Peres, J. M. B. L. dos Santos, J. Nilsson, F. Guinea, A. K. Geim, and A. H. C. Neto, Phys. Rev. Lett. **99**, 216802 (2007).
[19]J. Berezovsky, M. F. Borunda, E. J. Heller, and R. M. Westervelt, Nanotechnology **21**, 274013 (2010).
[20]J. Berezovsky and R. M. Westervelt, Nanotechnology **21**, 274014 (2010).
[21]L. Ressier and V. L. Nader, Nanotechnology **19**, 135301 (2008).
[22]G. M. Rutter, S. Jung, N. N. Klimov, D. B. Newell, N. B. Zhitenev, and J. A. Stroscio, Nat. Phys. **7**, 649 (2011).
[23]E. Palleau, L. Ressier, Ł. Borowik, and T. Mélin, Nanotechnology **21**, 225706 (2010).
[24]Note that a range of values for P are used in the literature (see, for example, Refs. 17, 26, 27); however, n_i is insensitive to P. Increasing P by 20% changes $E_F(r)$ by around 20%, but $n_i(r)$ by less than 1%.
[25]In a simplified 1D model in which E_g is neglected, we can calculate the induced charge density analytically. If a metallic tip is at a height h above the graphene which is on a thickness t of SiO_2 (permittivity $\epsilon_0\epsilon_r$) then $\sigma_i = \epsilon_0 V_T/(h + 1/\eta + \epsilon_r h/(\eta t))$ is the charge density in the bilayer, while $\sigma_{ml} = \epsilon_0(V_T/h + \kappa^2/2 - \kappa\sqrt{V_T/h + \kappa^2/4})$ is the density induced in a monolayer. Here, $\eta = e^2\gamma_1/(\pi P^2\epsilon_0)$ and $\kappa^2 = (t/h + \epsilon_r)^2 (\pi P^2\epsilon_0)/(e^3 t^2)$. When $h = 20$ nm and $t = 300$ nm, σ_{ml} is within 6% of σ_i if $V_T \geq 1$ V.
[26]R. Saito, M. S. Dresselhaus, and G. Dresselhaus, *Physical properties of carbon nanotubes*, Imperial College Press (1998).
[27]A. H. Castro Neto, F. Guinea, N. M. R. Peres, K. S. Novoselov, and A. K. Geim, Rev. Mod. Phys. **81**, 109–162 (2009).